New Journal of Physics
The open access journal at the forefront of physics
Deutsche Physikalische Gesellschaft DPG | IOP Institute of Physics

Fast Track Communication

Nonlinear spectroscopy of controllable many-body quantum systems

Manuel Gessner[1,2], Frank Schlawin[1,3], Hartmut Häffner[2], Shaul Mukamel[3] and Andreas Buchleitner[1]

[1] Physikalisches Institut, Albert-Ludwigs-Universität Freiburg, Hermann-Herder-Straße 3, 79104 Freiburg, Germany
[2] Department of Physics, University of California, Berkeley, California 94720, USA
[3] Department of Chemistry, University of California, Irvine, California 92697, USA
E-mail: manuel.gessner@physik.uni-freiburg.de and frank.schlawin@physik.uni-freiburg.de

Received 1 July 2014
Accepted for publication 1 September 2014
Published 19 September 2014

New Journal of Physics **16** (2014) 092001
doi:10.1088/1367-2630/16/9/092001

Abstract

We establish a novel approach to probing spatially resolved multitime correlation functions of interacting many-body systems, with scalable experimental overheads. Specifically, designing nonlinear measurement protocols for multi-dimensional spectra in a chain of trapped ions with single-site addressability enables us, for example, to distinguish coherent from incoherent transport processes, to quantify potential anharmonicities, and to identify decoherence-free subspaces.

Keywords: nonlinear spectroscopy, trapped ions, quantum optics

1. Introduction

To unravel the spectral and dynamical properties of composite quantum systems of increasing complexity constitutes an indispensable prerequisite for robust control in diverse areas of modern quantum science, from quantum information processing [1–3] over photo-induced chemical reactions [4] to the primary processes of light–energy conversion in nature and

technology [5, 6]. A key ingredient of truly complex quantum systems are strong correlations over broadly distributed energy and time scales [7], which may lead to critical behavior or emergent phenomena and become manifest in such systems' dynamics [8, 9].

For a precise characterization of the latter, higher-order correlation functions need to be probed, which poses a formidable experimental challenge [10–12]. Much progress has been accomplished in this regard in ultrafast, multidimensional spectroscopy of molecular aggregates, where experiments are often carried out under extremely challenging conditions characterized by short time scales and tight spatial confinement [12, 13–15]. In cold-matter experiments, however, where complexity is constructed by controlled assembly of individual components [8, 16–20], Ramsey-type pump–probe techniques are still the preferred experimental tool to probe many-body dynamics [21].

In a Ramsey experiment, the system evolves through a coherent superposition of ground- and excited-states in a two-pulse sequence. Such experiments can resolve the energies of contributing excited states, as well as decoherence rates caused by environmental couplings; they are, however, restricted in their combined frequency–time resolution [12], and cannot resolve manifolds of higher excited states or the contribution of individual pathways. For this reason, in chemical physics, one typically employs four-pulse sequences combined with a phase-dependent selection of quantum pathways to resolve involved transport processes, exciton couplings, and conformational changes in large molecular aggregates, such as photosynthetic complexes.

In this paper we combine this systematic construction of measurement protocols of higher-order correlation functions with the extraordinary control and, in particular, the single-site addressability of cold-matter systems [1, 22, 23]. We elaborate how our general formalism provides unmatched possibilities for the direct experimental assessment of spatially resolved multitime correlation functions, in experiments that rely on current trapped-ion technology. In particular, second- and fourth-order signals will be defined to monitor intricate dynamical features in the vibrational and electronic degrees of freedom.

2. Nonlinear measurement protocols

Inspired by multidimensional optical spectroscopy, we develop a general formalism to systematically construct nonlinear measurement protocols in quantum many-body systems using a diagrammatic theory. To provide physical intuition, we consider the example of vibrational degrees freedom in a chain of N ions in a linear trap. However, the obtained theoretical formalism is completely general and independent of the system or degree of freedom.

The ion-trap potential can be characterized by trap frequencies (ν_x, ν_y, ν_z), with the confinement much stronger in the transverse than in the axial direction $(\beta := \nu_z^2/\nu_x^2 \ll 1)$[4]. Transverse vibrations along the x-direction can then be described by a tight-binding Hamiltonian of local phonons including a tunneling term [24],

[4] We assume that the harmonic confinement along the two uncoupled transverse directions is of the same order of magnitude, i.e., $\nu_x \approx \nu_y$ [24].

$$H = \sum_{i=1}^{N} \omega_i^0 a_i^\dagger a_i + \sum_{i<j} t_{ij}\left(a_i^\dagger a_j + a_j^\dagger a_i\right), \tag{1}$$

where $a_i^\dagger$ denotes the creation operator for a local phonon at site i, $a_i^\dagger|0\rangle = |1_i\rangle$. The local trap frequencies and the coupling matrix can be microscopically derived as [24]

$$\omega_i^0/\nu_x = 1 - \frac{\beta}{2}\sum_{j\neq i}\frac{1}{\left|u_i^0 - u_j^0\right|^3}, \tag{2}$$

$$t_{ij}/\nu_x = \frac{\beta}{2}\frac{1}{\left|u_i^0 - u_j^0\right|^3}, \tag{3}$$

with $u_i^0 = z_i^0/l_0$, where z_i^0 denotes the ion's equilibrium positions, and a typical length scale is given by $l_0^3 = e^2/(m\nu_z^2)$ [25]. An additional anharmonic potential $U\sum_i a_i^{\dagger 2} a_i^2$ with tunable strength U can be induced by a standing electromagnetic wave, effectively generating a Bose–Hubbard model with long-range couplings [24].

The basic building blocks for multidimensional spectroscopic protocols are excitation and readout schemes. A vibrational excitation of the form $D_j(\alpha e^{i\phi}) \approx \mathbb{1} + \alpha e^{i\phi} a_j^\dagger - \alpha e^{-i\phi} a_j$ can be generated by suitable, perturbative pulse sequences [26, 27], where $\alpha \ll 1$, and ϕ can be controlled through the pulse parameters. The superoperator $\mathcal{V}_j(\phi)[\rho] = D_j(\alpha e^{i\phi})\rho D_j^\dagger(\alpha e^{i\phi})$ describes the corresponding change of the density matrix induced by this weak interaction. In the course of this paper, we consider the impulsive limit for the interaction $\mathcal{V}$, which means that the duration of the light pulses is much shorter than the time scale of the vibrational dynamics. This is justified since the characteristic time scale of the Hamiltonian evolution can be adjusted by controlling the distance between neighboring ions via the parameter β [24]. Excitations of local phonons can be read out via the observable $A_j = \sum_{n_j=1}^{\infty} \sin^2\left(\sqrt{n_j}\,\pi/2\right)|n_j\rangle\langle n_j|$ (j labels the measured ion), which is accessible by mapping the vibrational population onto the ion's electronic state [28] (see appendix A).

Using these ingredients, multidimensional spectra are obtained by scanning the time delays between a sequence of pulses and detecting the observable A_j. After a series of m interactions on the ions $i_1,\ldots,i_m$, the signal is given by

$$S^{(m)}_{i_1,\ldots,i_m;\,j}(t_1,\ldots,t_m) = \left\langle A_j \right\rangle = \mathrm{Tr}\left\{A_j \rho^{(m)}_{i_1,\ldots,i_m}(t_1,\ldots,t_m)\right\}, \tag{4}$$

where the expectation value is taken with respect to the non-equilibrium density matrix created by a succession of short, impulsive interaction events and unperturbed time evolution,

$$\rho^{(m)}_{i_1,\ldots,i_m}(t_1,\ldots,t_m) = \mathcal{G}(t_m)\mathcal{V}_{i_m}(\phi_m)\ldots\mathcal{G}(t_1)\mathcal{V}_{i_1}(\phi_1)[\rho(0)]. \tag{5}$$

The latter is described by the Green's function $\mathcal{G}(t) = \exp \mathcal{L}t$, where $\mathcal{L}$ denotes the Liouville superoperator [12, 29], which we assume is time-independent: $\mathcal{L}[\rho] = -i[H,\rho] + \sum_i (L_i \rho L_i^\dagger - \frac{1}{2}\{L_i^\dagger L_i, \rho\})$. Different Lindblad operators L_i [29] can be simulated in trapped-ion systems [30–32].

These signals constitute a generalization of Ramsey spectroscopy, and provide the possibility to distinguish the contributions of individual quantum pathways. To see this, note that each time an excitation is created or destroyed due to the interaction $\mathcal{V}_{i_k}(\phi_k)$, the phase ϕ_k of the kth pulse is imprinted on the quantum state. Hence, different contributions to the total signal can be distinguished by their dependence on these phases. One can exploit this to post-

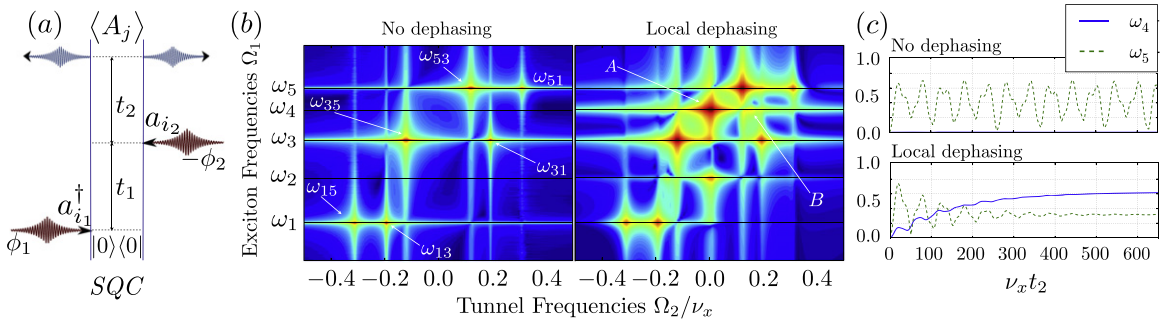

Figure 1. The single quantum coherence (SQC) signal unveils space- and time-resolved exciton evolution. (a) The Feynman diagram describing $S^{(\mathrm{SQC})}_{i_1,\,i_2;\,j}$ depicts those contributions to the impulsive excitations (red arrows) $\mathcal{V}_j(\phi)$, which imprint the phase label $\phi_1 - \phi_2$. Blue arrows indicate readout (see appendix B for an interpretation of the diagrams). (b) $|S^{(\mathrm{SQC})}_{1,\,1;\,3}(\Omega_1, \Omega_2)|$ reveals the contributing exciton spectrum (along Ω_1) and tunneling rates along Ω_2, for unitary dynamics (left), and under additional local dephasing with strength $\gamma = 0.01\nu_x$ (right). The signals are rescaled by arcsinh to highlight small features. (c) Time-resolved exciton transport can be read off from $|S^{(\mathrm{SQC})}_{1,\,1;\,3}(\Omega_1, t_2)|$ for $\Omega_1 = \omega_4$ (blue, solid line) and for $\Omega_1 = \omega_5$ (red, dashed line). The emergence of a signal at $\Omega_1 = \omega_4$ under the influence of noise indicates incoherent exciton transport. At transient times, coherent exciton couplings can be observed as well. For $\beta = 0.1$, diagonalization of the Hamiltonian (1) yields $\omega_1 = 0.69\nu_x$ and $\omega_5 = \nu_x$.

select signals pertaining to certain pathways with distinct combinations of coherences and populations: To this end one employs the phase cycling protocol originally developed in nuclear magnetic resonance [10]. It is implemented by repeating the experiment for a small discrete set of phases followed by Fourier analysis [10, 33]. Individual pathways can be represented by Feynman diagrams [12], which offer an intuitive interpretation of the signals (see also figure 1(a)). Further information on coherent pathways and their selection via phase cycling can be found in appendix B.

Let us stress that the way such signals are obtained in controlled quantum systems holds considerable advantages over related methods, such as phase-matched heterodyne ensemble spectroscopy of bulk materials [11, 12] or phase-sensitive fluorescence measurements [34], e.g., of single molecules [33]. Specifically, we point out three key differences between these methods and the approach proposed here.

- The first consists of the ability to create localized excitations due to the micrometer separation of the ions, which induces superpositions of a multitude of eigenstates with a single interaction. This is not possible, for instance, when working on molecular aggregates, where interacting chromophores are separated only by few nanometers, two orders of magnitude below the diffraction limit of optical light.
- Second, since artificial quantum systems, as considered in the present manuscript, are typically well isolated from the environment, the induced excitations do not decay naturally within the relevant experimental time scales [1]. Instead, the described fluorescence signal must be induced externally via coupling to a short-lived state, providing full control over the delay between readout and the final interaction. Direct field

measurements of the Raman scattered light are not suitable for these single quantum systems due to the insufficient number of scattered photons. This is in stark contrast to fluorescence measurements in molecular systems, where fluorescence signals are created by spontaneous decay after a random time, and heterodyne measurements of stimulated emission, which is induced immediately following the last excitation. Therefore, methods that were developed for phase-matched heterodyne electronic spectroscopy cannot be implemented straightforwardly and instead must be adjusted to the current fluorescence-based situation. However, as we will show later in this manuscript, analogs of well-known measurement protocols from electronic two-dimensional (2D) spectroscopy can be defined and interpreted similarly.

- Third, aside from strong spatial confinement, experiments on molecular aggregates are also characterized by extremely challenging time scales. For instance, typical time scales for energy transport and coherence decay on photosynthetic complexes are on the order of picoseconds [5, 12]. These parameters render precise experimental control of such molecular aggregates extremely demanding. In contrast, quantum optical experiments, such as trapped ions, allow the study of energy transport under well-controlled conditions on microsecond time scales with milliseconds of coherent dynamics [26, 27].

Let us also briefly comment on the difference between single-shot experiments on an ensemble of systems in bulk and experiments on single quantum systems, which are repeated many times to obtain a statistically relevant sample of results. In the latter case, ensemble averaging over slightly fluctuating conditions leads to decoherence effects whose phenomenology is similar to that experienced in bulk materials. In ion-trap experiments, those effects are especially relevant in the context of quantum computation, and consequently have been analyzed thoroughly [35]. For the application of the proposed methods, these effects do not pose a problem, as demonstrated, for instance, by the successful implementation of related methods with single molecules [33].

Making use of the advantages discussed above, we can now design nonlinear signals to target specific dynamical and spectral features of engineered quantum matter systems. Current quantum optical experiments struggle with the efficient analysis of long-range coherences, which are responsible for notoriously elusive quantum critical phenomena [36], and whose role is also currently debated in quantum transport processes [15] which in turn may be studied in quantum simulations [20]. Moreover, in light of their increasing complexity, appropriate methods to certify and diagnose quantum computations are lacking—in particular, for the unambiguous identification of sources of error, such as anharmonic corrections to the trap potential and the precise characterization of detrimental effects induced by external environments [35]. In the following, we show how nonlinear spectroscopy is able to improve on this situation, by demonstrating a selection of applications for examples of second- and fourth order signals.

3. Applications

3.1. Coherent and incoherent phonon transport

As a first application, we scrutinize the role of quantum coherence for phonon transport in an ion chain via a second-order signal that monitors the space- and time-resolved spectral

decomposition of a local excitation. To this end, we introduce the single quantum coherence (SQC) signal,

$$S^{(\mathrm{SQC})}_{i_1,\,i_2;\,j}(t_1,\,t_2) = \mathrm{Tr}\left\{ A_j \mathcal{G}(t_2)\Big[\,\mathcal{G}(t_1)\Big[\,a^{\dagger}_{i_1}\rho(0)\Big]a_{i_2}\Big]\right\} \tag{6}$$

which is extracted by phase cycling with respect to the phase $\phi_1 - \phi_2$ (figure 1(a)) from the total second-order signal $S^{(2)}_{i_1,\,i_2;\,j}(t_1,\,t_2)$. It contains time-correlation functions whose spatial resolution is controlled by the choice of excitation and readout pulses: the first tunable delay t_1 between the excitation pulses at ions i_1 and i_2 and a second tunable delay t_2 before readout at ion j are scanned. To unveil spectral properties, we Fourier-transform the signal with respect to one or both time delays, e.g.,

$$S^{(\mathrm{SQC})}_{i_1,\,i_2;\,j}\left(\Omega_1,\,\Omega_2\right) = \int_0^{\infty} dt_1 \int_0^{\infty} dt_2\; e^{i(\Omega_1 t_1 + \Omega_2 t_2)} S^{(\mathrm{SQC})}_{i_1,\,i_2;\,j}(t_1,\,t_2). \tag{7}$$

In figure 1, we simulate [37] SQC signals for a chain of five ions initialized in their individual ground states $|0\rangle$ with a confinement parameter of $\beta = 0.1$. The first two pulses create vibrational excitations at the left-most ion, i.e., $i_1 = i_2 = 1$, which are then probed, after interaction-induced propagation, at the central ion, $j = 3$. For the interpretation of the spectrum, it is most instructive to represent the local excitations in terms of single exciton states (energy eigenstates of the chain) $|e_j\rangle$, e.g., $a_1^{\dagger}|0\rangle = |1_1\rangle = \sum_j c_{1j}|e_j\rangle$, which evolve with their respective eigenfrequencies ω_j. We emphasize that the index j now refers to an eigenstate of the chain, i.e., we now work in the exciton basis—in contrast to equation (1), where the Hamiltonian was described on a local-site basis. Since the first pulse induces the coherence $|1\rangle\langle 0|$, which is selected via its phase signature ϕ_1 (see figure 1(a)), the Fourier transform with respect to the first time delay t_1 reveals the single exciton frequencies ω_j. During t_2, the contributions with the phase label $\phi_1 - \phi_2$ involve coherences between distinct excitons, such that the Fourier transform of t_2 reveals the energy differences $\omega_{ij} = \omega_i - \omega_j$ (figure 1(b)). As we can easily see, these determine the periods at which an excitation coherently tunnels between the ions: the probability for a phonon localized on ion a to tunnel to ion b at a time t is given by $p_{ab}(t) = |\langle 1_b|e^{-iHt}|1_a\rangle|^2 = \sum_{ij} c_{ij} e^{-i\omega_{ij}t}$, with $c_{ij} = \langle 1_b|e_i\rangle\langle e_i|1_a\rangle\langle 1_a|e_j\rangle\langle e_j|1_b\rangle$. We will therefore denote the frequency differences ω_{ij} as tunnel frequencies. We remark here that the measurement protocol that reveals these frequencies only requires two localized excitation pulses and one readout pulse, *independently* of the length of the chain.

In the right panel of figure 1(b), we now add local dephasing, described by $L_i = \sqrt{\gamma}\, a_i^{\dagger} a_i$ [30, 31]. Coupling to the environment causes additional transitions, which induce incoherent transport. To understand this, we plot $|S^{(\mathrm{SQC})}_{1,\,1;\,3}(\Omega_1,\,t_2)|$ in figure 1(c), which displays the evolution of the initial state's frequency components during t_2 and thereby allows one to monitor the time-resolved exciton transport. Without dephasing (top panel), there is no signal at ω_4, since the associated breathing mode leaves the central ion immobile [25], and is therefore not detected by local readout. However, in the presence of local dephasing, the breathing mode is incoherently coupled to other modes, which do have a finite amplitude at the central ion. Thus, the bottom panel of figure 1(c) shows the emergence of a signal at ω_4 with increasing t_2. We observe progressively incoherent (non-oscillatory) transport, leading to a pronounced 2D signal at $(\Omega_1,\,\Omega_2) = (\omega_4,\,0)$ (peak A). The transient oscillations on top are due to short-lived coherences between the excitons $|e_4\rangle$ and $|e_2\rangle$, and give rise to another, weak 2D signal at $(\omega_4,\,\omega_{42})$ (peak B). Thus, our local readout scheme provides full information on spatially

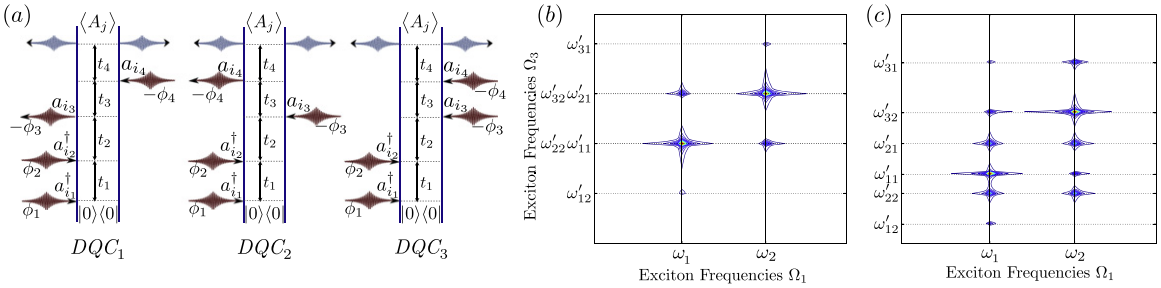

Figure 2. The double quantum coherence (DQC) signal is ideally suited for a spectral characterization of trap anharmonicities and the identification of excitation pathways to the double exciton manifold. (a) The three diagrams with phase signature $\phi_1 + \phi_2 - \phi_3 - \phi_4$ constitute the DQC signal. (b) In a harmonic trap ($U = 0$), $|S^{(\mathrm{SQC})}_{0000;\,0}(\Omega_1, t_2 = 0, \Omega_3, t_4 = 0)|$ displays degenerate double excitons. (c) A symmetry-breaking anharmonic correction ($U = -0.025\nu_x$) lifts these degeneracies and creates new pathways, as revealed, e.g., by the peak at (ω_1, ω'_{31}). The Ω_3 axis is the same in plots (b) and (c); however, the resonances are shifted in panel (c), due to the anharmonicity. Both plots simulate signals of two ions with $\beta = 0.1$, leading to $\omega_1 = 0.95\nu_x$ and $\omega_2 = \nu_x$.

resolved transport and on the coherently or incoherently populated transporting eigenmodes of the chain.

3.2. Detection of anharmonicities

The second order signal employed in our example above can only probe excitonic states within the single excitation manifold (due to the very structure of the impulsive interaction $\mathcal{V}_j(\phi)$), and is therefore unsuitable to detect any anharmoniticity of the phonon spectrum. For the latter purpose, we need to probe the *double* excitation manifold, and, hence, to find an appropriate fourth-order signal. Such an observable is given by the double quantum coherence (DQC), which has been successfully employed to probe electronic correlations in molecules [38] (see also [39]). For our present purposes, we define the analogous fluorescence-based signal, consisting of the four-pulse pathways with phase signature $\phi_1 + \phi_2 - \phi_3 - \phi_4$ (figure 2(a)). The first two pulses create a double exciton (two-phonon) state $|f_i\rangle$, which is subsequently probed by the third and fourth pulses. During t_1, the created coherence evolves with frequencies ω_i, whereas during t_3, it oscillates with either ω_i (DQC_1) or $\omega'_{ij} = \omega_{f_i} - \omega_j$ (DQC_2 and DQC_3), where ω_{f_i} are the eigenfrequencies of the double exciton states $|f_i\rangle$. A Fourier transform with respect to the time delays t_1 and t_3 reveals signal contributions at ω_i and ω'_{ij}, along Ω_1 and Ω_3, respectively. In the following, the single and double exciton energies ω_i and ω_{f_i} are labeled in ascending order, i.e., $\omega_1 < \omega_2 < \ldots$, and $\omega_{f_1} < \omega_{f_2} < \ldots$, respectively.

Let us consider the example $N = 2$, where all pulses are applied to the same ion and the times t_2 and t_4 are kept at zero. Note that, as pointed out in the introduction, and in contrast to other methods, this approach allows us to scan the time interval t_4 as well, which can be extremely useful for studies of, for instance, population decay. For the detection of anharmonicities, however, only the time intervals t_1 and t_3 need to be considered. Since for vanishing anharmonicity, $U = 0$, the energy of each double exciton state $|f_i\rangle$ is given by the sum of two single exciton energies, $\omega_{f_i} = \omega_j + \omega_k$, transitions so that ω'_{11} and ω'_{22} coincide in

figure 2(b). Moreover, peaks involving $\omega_{f_j} = 2\omega_i$ may only be observed along $\Omega_1 = \omega_i$ since only if the first pulse excites $|e_i\rangle$, the second pulse can promote the system into $|f_j\rangle$. For instance, we do not observe a peak at (ω_1, ω'_{31}), since $\omega_{f_3} = 2\omega_2$.

When we add anharmonicity to the system ($U \neq 0$), two effects can be observed [figure 2(c)]: First, degeneracies are lifted, and the signals at ω'_{11} and ω'_{22} can be resolved. Second, the anharmonicity U perturbs the symmetry of double excitons. This opens up new excitation pathways, e.g., $|f_3\rangle$ can be accessed via $|e_1\rangle$, creating a signal at (ω_1, ω'_{31}). The strength of the anharmonicity U can be inferred by comparing the distance of the ω'_{ij}-transitions to the possible harmonic transitions, which in turn can be recovered from single-exciton frequencies along the Ω_1-axis.

3.3. 2D lineshapes

So far, we have demonstrated how to assess spectral properties of the *vibrational* degree of freedom of the ion chain. However, each ion also carries an *electronic* degree of freedom, which can be treated as a spin-1/2 system. The vibrational modes then mediate the coupling between the different spins. Applications of this type of interactions for quantum information purposes potentially suffer from the detrimental influence of environmental noise, what renders a precise characterization of decoherence mechanisms highly desirable in any such experiment. In our last example to illustrate the versatility of nonlinear spectroscopic techniques in combination with single-site resolution, we demonstrate how the line shape of a 2D signal can reveal the nature and strength of the environmental coupling and identify a decoherence-free subspace. We further show how this can be used to certify the fidelity of Bell-state generation.

The formalism for the construction of nonlinear signals introduced before can be readily adapted to other degrees of freedom by identifying appropriate excitation and readout schemes. For spins, we consider the interaction $\mathcal{V}_j(\phi)\rho = U_j(\phi)\rho U_j^\dagger(\phi)$, where $U_j(\phi) = \alpha\mathbb{1}^{(j)} + \beta(e^{i\phi}\sigma_+^{(j)} - e^{-i\phi}\sigma_-^{(j)})$, $|\alpha|^2 + |\beta|^2 = 1$, can be generated by a focused resonant laser pulse on spin j [40], with $\sigma_\pm^{(j)} = (\sigma_x^{(j)} \pm i\sigma_y^{(j)})/2$, and $\sigma_{x,\,y,\,z}^{(j)}$ the Pauli matrices of spin $j = 1,2$. We choose the readout observable $A_j = \sigma_z^{(j)}$, corresponding to a measurement of the population at spin j [40].

The effective spin–spin interaction is described by the Mølmer–Sørensen Hamiltonian, which for two spins takes the form $H_{\mathrm{MS}} = (\Omega/2)\sigma_x^{(1)} \otimes \sigma_x^{(2)}$. The two ions are initialized in their electronic ground state $|00\rangle$, and all excitations and the readout are carried out on the same spin. One can readily predict four resonances at $(\Omega_1, \Omega_2) = \pm(0, \Omega)$ and $\pm(\Omega, \Omega)$, generated by coherences of Bell states $\{|\Psi^\pm\rangle, |\Phi^\pm\rangle\}$, which are eigenstates of H_{MS} with eigenvalues $\pm\Omega/2$ [41]. Without dissipation, all four peaks are delta peaks, yet the coupling to an environment can broaden them and gives rise to distinct 2D lineshapes. Figure 3(a) compares the lineshape of the (Ω, Ω)-peak under the effect of a local noise process, described by the two Lindblad operators $L_{\mathrm{ld}}^{(j)} = \sqrt{\gamma}\sigma_z^{(j)}$, $j = 1,2$, with the lineshape under correlated dephasing described by $L_{\mathrm{cd}} = \sqrt{\gamma}\sigma_z^{(1)} \otimes \sigma_z^{(2)}$. Local dephasing broadens the resonances equally along both frequency axes, whereas collective dephasing only affects the width along Ω_1. The selected quantum pathway evolves in the coherence $|\Psi^\pm\rangle\langle\Psi^\mp|$ during t_2, which is part of a decoherence-free subspace [42]. For local dephasing, the peak width along Ω_1 allows us to infer the error probability of the corresponding gate $U_{\mathrm{MS}} = \exp(-iH_{\mathrm{MS}}\pi/2\Omega)$, since both of these quantities scale approximately linearly with the dephasing strength γ for $\gamma < 0.1\Omega$ (figure 3(b)). The error

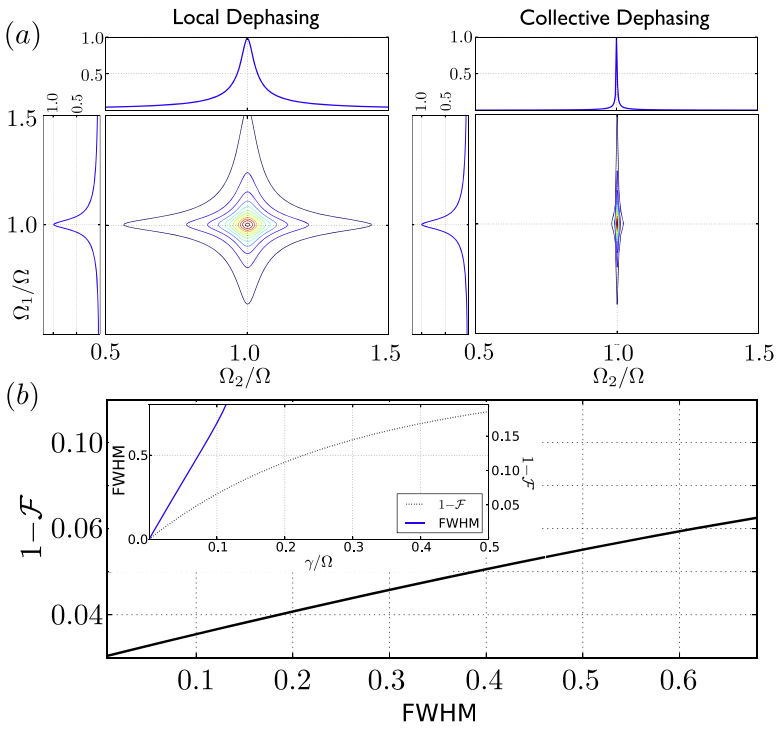

Figure 3. Decoherence mechanisms can be identified and quantified via 2D lineshapes. (a) (Ω, Ω)-signal of $|S^{(\mathrm{SQC})}_{1,\,1;\,1}(\Omega_1, \Omega_2)|$ as read off from two spins initially prepared in the state $|00\rangle$ and subject to the Mølmer–Sørensen interaction. The 2D lineshapes clearly distinguish between local and collective dephasing processes. Only under collective dephasing, the system evolves in a decoherence-free subspace during t_2, as manifest in the delta-shaped signal along Ω_2. (b) For weak local dephasing ($\gamma < 0.1\Omega$), the full-width-half-maximum (FWHM) along Ω_1 scales approximately linearly with the corresponding Mølmer–Sørensen gate error $1 - \mathcal{F}$, since both relate to the strength of the noise γ (inset).

probability is quantified via the fidelity $\mathcal{F} = \sqrt{\langle 00|U^{\dagger}_{\mathrm{MS}}\rho_{\gamma}U_{\mathrm{MS}}|00\rangle}$ as $1 - \mathcal{F}$, where $\rho_{\gamma} = \mathcal{G}(\pi/2\Omega)[|00\rangle\langle 00|]$ denotes the state at the outcome of the noisy gate.

4. Conclusion

We have presented a powerful method to probe spatially resolved multitime correlation functions for the investigation of complex non-equilibrium dynamics and discussed experimental realizations with trapped ions. Our methods generalize previous Ramsey-type techniques inasmuch as they allow for the construction of pulse sequences of arbitrary order and phase-coherently select the contribution of individual quantum pathways.

Our diagrammatic theory provides an intuitive description as well as a new language for cold matter experiments and can be readily extended to include recent developments from nonlinear spectroscopy, such as pulse-shaping and optimal control theory [43, 44]. We envision that, beyond trapped ions, implementations with cold Rydberg gases [45, 46] and spins of neutral atoms in optical lattices are within experimental reach [21, 23].

We thereby provide a versatile toolbox for controlled quantum systems, opening up a wide range of possibilities to systematically study many-body effects in complex quantum systems, such as the survival of coherences under different environmental and internal couplings, as well as the role of excitonic states in quantum transport processes. The number of pulses required to probe a certain multipoint correlation function is independent of the system size, which renders this method scalable in the limit of increasing particles. This establishes an important step towards the experimental certification of quantum effects in large-scale quantum devices.

Acknowledgements

We would like to thank Michael Ramm for helpful discussions. MG and FS thank the German National Academic Foundation for support. SM gratefully acknowledges the support of the National Science Foundation through grant no. CHE-1058791, and the Chemical Sciences, Geosciences and Biosciences Division, Office of Basic Energy Sciences, Office of Science, US Department of Energy. This work was supported by the NSF CAREER Program grant no. PHY 0955650. The article processing charge was funded by the open access publication fund of the Albert Ludwigs University Freiburg.

Appendix A. Fluorescence readout of phonon populations

Populations of the vibrational degree of freedom can be probed using sideband transitions, i.e., by driving the electronic resonance with a laser detuning that corresponds to the trap frequency. Specifically, addressing the first red sideband (with a red detuning of $-\nu_x$) of an electronic transition between two states $|\uparrow\rangle$ and $|\downarrow\rangle$ with a pulse duration $t = \pi/\eta\Omega$ maps an initial state $|\downarrow, n\rangle$ to

$$U_{-1}(\pi)|\downarrow, n\rangle = \cos\left(\sqrt{n}\frac{\pi}{2}\right)|\downarrow, n\rangle + \sin\left(\sqrt{n}\frac{\pi}{2}\right)|\uparrow, n-1\rangle, \tag{A.1}$$

with the Rabi frequency Ω of the carrier transition (resonant to the electronic levels); we have also neglected contributions of the order η^2, where η denotes the Lamb–Dicke parameter [40]. This pulse is followed by fluorescence readout of the electronic excitation, which can be done conveniently and with high efficiency using a short-lived, excited electronic state coupled only to the electronic ground state, but not to the excited state [40]. The probability of detecting the ion in the excited state is then given by $|\sin(\sqrt{n}\,\pi/2)|^2$, and this measurement sequence is thus equivalent to effectively measuring the motional observable

$$A = \sum_{n=0}^{\infty} \sin^2\left(\sqrt{n}\frac{\pi}{2}\right)|n\rangle\langle n|. \tag{A.2}$$

This sequence can be applied to single ions in a tight laser focus of sufficient intensity, to probe local vibrational excitations.

Appendix B. Nonlinear spectroscopy and phase cycling

To obtain multidimensional spectra, one applies a series of pulses with well-defined phase relations and tunable time delays to the system of interest. The signal is measured as a function of the time delays between the pulses. Considering, for instance, an excitation of the form

$D_j(\alpha e^{i\phi}) \approx \mathbb{I} + \alpha e^{i\phi} a_j^\dagger - \alpha e^{-i\phi} a_j$, the created coherences will carry the phase-shift $e^{\pm i\phi}$. All the contributions in a sequence of pulses can be represented by Feynman ladder diagrams, each one representing one excitation pathway with a characteristic phase signature (the combined phase shift of all pulses in the applied sequence), as for instance in figures 1(a) and 2(a). The diagrams are to be read as follows:

- Time runs from bottom to top, the left vertical depicts the evolution of the *ket*, and the right one the evolution of the *bra* side of the density matrix.
- Each excitation (de-excitation) is described by an arrow pointing towards (away from) the density matrix. Each de-excitation adds a factor (-1) to the overall sign of the diagram.
- To yield a signal, the diagram has to end up in an excited state population when the fluorescence is collected.

The total signal is described by a coherent superposition of all pathways. A complete pedagogical introduction to this formalism is beyond the scope of the current paper, but can be found in a recent review [47], which is specifically written to appeal to quantum opticians, as well as to be appropriate for standard textbooks [11, 12].

Phase cycling is a post-processing method that allows us to extract the contribution of subsets of pathways from the total signal, by exploiting their dependence on the phases [10]. To this end, the phases ϕ_i of the individual pulses have to be scanned over a discrete set of values.

For example, consider a pulse sequence, where the phase signatures $k\Delta\phi$, $k = 0, \pm 1, ..., \pm k_{\max}$ occur, where in a perturbative treatment of the low-intensity pulses as considered above, $k_{\max}$ can typically be assumed to be small (i.e., $k_{\max} = 1$ or 2). From the total signal, which decomposes into a sum of terms with different phase shifts,

$$S^{(2)}(\Delta\phi) = \sum_{k=-k_{\max}}^{k_{\max}} S_k^{(2)} e^{ik\Delta\phi}, \tag{B.1}$$

we can extract the complex-valued terms $S_k^{(2)}$ using an inverse discrete Fourier transform:

$$S_k^{(2)} = \frac{1}{2k_{\max} + 1} \sum_{j=0}^{2k_{\max}} S^{(2)}\left(\delta\phi_j\right) e^{-ik\delta\phi_j}, \tag{B.2}$$

with $\delta\phi_j = 2\pi j/(2k_{\max} + 1)$. Thus, by scanning the phase shifts over a specifically chosen set, followed by an inverse discrete Fourier analysis of the obtained spectra, it is possible to experimentally select the contribution of individual pathways.

References

[1] Häffner H, Roos C F and Blatt R 2008 Quantum computing with trapped ions *Phys. Rep.* **469** 155

[2] Tillmann M *et al* 2013 Experimental boson sampling *Nat. Photonics* **7** 540

[3] Crespi A *et al* 2013 Integrated multimode interferometers with arbitrary designs for photonic boson sampling *Nat. Photonics* **7** 545

[4] Assion A *et al* 1998 Control of chemical reactions by feedback-optimized phase-shaped femtosecond laser pulses *Science* **282** 919

[5] Scholes G D, Fleming G R, Olaya-Castro A and van Grondelle R 2011 Lessons from nature about solar light harvesting *Nat. Chem.* **3** 763

[6] Clarke T M and Durrant J R 2010 Charge photogeneration in organic solar cells *Chem. Rev.* **110** 6736

[7] Goulielmakis E *et al* 2010 Real-time observation of valence electron motion *Nature* **466** 739
[8] Madroñero J *et al* 2006 Quantum chaos, transport, and control–in quantum optics *Adv. At., Mol., Opt. Phys.* **53** 33
[9] Evers F and Mirlin A D 2008 Anderson transitions *Rev. Mod. Phys.* **80** 1355
[10] Ernst R R, Bodenhausen G and Wokaun A 1987 *Principles of Nuclear Magnetic Resonance in One and Two Dimensions* (Oxford: Oxford University Press)
[11] Hamm P and Zanni M 2011 *Concepts and Methods of 2D Infrared Spectroscopy* (Cambridge: Cambridge University Press)
[12] Mukamel S 1999 *Principles of Nonlinear Optical Spectroscopy* (Oxford: Oxford University Press)
[13] Schlau-Cohen G S, Ishizaki A and Fleming G R 2011 Two-dimensional electronic spectroscopy and photosynthesis: fundamentals and applications to photosynthetic light-harvesting *Chem. Phys.* **386** 1
[14] Milota F, Sperling J, Nemeth A, Mančal T and Kauffmann H F 2009 Two-dimensional electronic spectroscopy of molecular excitons *Acc. Chem. Res.* **42** 1364
[15] Engel G S *et al* 2007 Evidence for wavelike energy transfer through quantum coherence in photosynthetic systems *Nature* **446** 782
[16] Blatt R and Roos C F 2012 Quantum simulations with trapped ions *Nat. Phys.* **8** 277
[17] Bloch I, Dalibard J and Zwerger W 2008 Many-body physics with ultracold gases *Rev. Mod. Phys.* **80** 885
[18] Saffman M, Walker T G and Mølmer K 2010 Quantum information with Rydberg atoms *Rev. Mod. Phys.* **82** 2313
[19] Britton J W *et al* 2012 Engineered two-dimensional Ising interactions in a trapped-ion quantum simulator with hundreds of spins *Nature* **484** 489
[20] Bermudez A, Bruderer M and Plenio M B 2013 Controlling and measuring quantum transport of heat in trapped-ion crystals *Phys. Rev. Lett.* **111** 040601
[21] Knap M *et al* 2013 Probing real-space and time-resolved correlation functions with many-body Ramsey interferometry *Phys. Rev. Lett.* **111** 147205
[22] Bakr W S *et al* 2010 Probing the superfluid-to-Mott insulator transition at the single-atom level *Science* **329** 547
[23] Weitenberg C *et al* 2011 Single-spin addressing in an atomic Mott insulator *Nature* **471** 319
[24] Porras D and Cirac J I 2004 Bose–Einstein condensation and strong-correlation behavior of phonons in ion traps *Phys. Rev. Lett.* **93** 263602
[25] James D F V 1998 Quantum dynamics of cold trapped ions with application to quantum computation *Appl. Phys.* B **66** 181
[26] Brown K *et al* 2011 Coupled quantized mechanical oscillators *Nature* **471** 196
[27] Harlander M *et al* 2011 Trapped-ion antennae for the transmission of quantum information *Nature* **471** 200
[28] Heinzen D J and Wineland D J 1990 Quantum-limited cooling and detection of radio-frequency oscillations by laser-cooled ions *Phys. Rev.* A **42** 2977
[29] Breuer H-P and Petruccione F 2007 *The Theory of Open Quantum Systems* (Oxford: Oxford University Press)
[30] Poyatos J F, Cirac J I and Zoller P 1996 Quantum reservoir engineering with laser cooled trapped ions *Phys. Rev. Lett.* **77** 4728
[31] Myatt C J *et al* 2000 Decoherence of quantum superpositions through coupling to engineered reservoirs *Nature* **403** 269
[32] Barreiro J T *et al* 2011 An open-system quantum simulator with trapped ions *Nature* **470** 486
[33] Hildner R, Brinks D and van Hulst N F 2011 Femtosecond coherence and quantum control of single molecules at room temperature *Nat. Phys.* **7** 172
[34] Lott G A *et al* 2011 Conformation of self-assembled porphyrin dimers in liposome vesicles by phase-modulation 2D fluorescence spectroscopy *Proc. Natl Acad. Sci.* **108** 16521
[35] Schindler P *et al* 2013 A quantum information processor with trapped ions *New J. Phys.* **15** 123012
[36] Blankenship R E 2009 *Molecular Mechanisms of Photosynthesis* (Oxford: Blackwell)

[37] Islam R *et al* 2013 Emergence and frustration of magnetism with variable-range interactions in a quantum simulator *Science* **340** 583
[38] Johansson J R, Nation P D and Nori F 2013 QuTiP 2: a python framework for the dynamics of open quantum systems *Comp. Phys. Comm.* **184** 1234
[39] Kim J, Mukamel S and Scholes G D 2009 Two-dimensional electronic double-quantum coherence spectroscopy *Acc. Chem. Res.* **42** 1375
[40] Nemeth A *et al* 2010 Double-quantum two-dimensional electronic spectroscopy of a three-level system: experiments and simulations *J. Chem. Phys.* **133** 094505
[41] Leibfried D, Blatt R, Monroe C and Wineland D 2003 Quantum dynamics of single trapped ions *Rev. Mod. Phys.* **75** 281
[42] Sørensen A and Mølmer K 1999 Quantum computation with ions in thermal motion *Phys. Rev. Lett.* **82** 1971
[43] Lidar D A, Chuang I L and Whaley K B 1998 Decoherence-free subspaces for quantum computation *Phys. Rev. Lett.* **81** 2594
[44] Voronine D, Abramavicius D and Mukamel S 2006 Coherent control of cross-peaks in chirality-induced two-dimensional optical signals of excitons *J. Chem. Phys.* **125** 224505
[45] Herek J L *et al* 2002 Quantum control of energy flow in light harvesting *Nature* **417** 533
[46] Fuhrmanek A, Bourgain R, Sortais Y R P and Browaeys A 2011 Free-space lossless state detection of a single trapped atom *Phys. Rev. Lett.* **106** 133003
[47] Günter G *et al* 2013 Observing the dynamics of dipole-mediated energy transport by interaction-enhanced imaging *Science* **342** 954
[48] Brańczyk A M, Turner D B and Scholes G D 2014 Crossing disciplines—a view on two-dimensional optical spectroscopy *Ann. Phys.* **526** 31